PERGAMON

International Journal of Heat and Mass Transfer 45 (2002) 4703–4711

International Journal of HEAT and MASS TRANSFER

www.elsevier.com/locate/ijhmt

Creeping flow of a polymeric liquid passing over a transverse slot with viscous dissipation

G.H. Wu *, Y.M. Lin

Department of Mechanical Engineering, National Cheng-Kung University, Tainan, Taiwan, ROC

Received 25 February 2001

Abstract

Numerical simulations for the non-isothermal flow of a nylon-6 fluid passing over a transverse slot with heat dissipation are considered with a differential-type non-isothermal White–Metzner model describing the non-Newtonian behavior of the melt. The results obtained in the study are computed by using the elastic–viscous split-stress finite element method incorporating the non-consistent streamline-upwind scheme. As a verification of the numerical scheme, the algorithm is first applied to compute the corresponding isothermal flow of the upper-convected Maxwell fluid, a special case of the melt, characterized by constant viscosity and relaxation time. Hole pressure was evaluated for various Deborah numbers (De), and compared with that derived from the Higashitani–Pritchard (HP) theory. The agreement between the two is found to be satisfactory for creeping flow in the De range for which the HP theory is valid. Subsequently, hole pressure and other flow characteristics were predicted. Furthermore, the effects of heat-transfer, shear-thinning, and slot geometry on hole pressure were also investigated.

1. Introduction

The flow of a polymeric or viscoelastic liquid between two parallel plates across a transverse slot, is considered as illustrated in Fig. 1. Pressure transducers mounted at points a and b show the readings of $P_a = (p_a - \tau^a_{yy})$ and $P_b = (p_b - \tau^b_{yy})$, respectively. The difference is called hole pressure (P_h) in the literature [1,2] and is defined by $P_h = P_b - P_a = (p_b - p_a) + (\tau^a_{yy} - \tau^b_{yy})$. For creeping Newtonian flow, this value equals to zero. But for polymeric fluids, we find $P_h > 0$. This is attributed to viscoelastic effects.

The understanding of such a flow is important for engineering applications and has attracted a great deal of attention in the literature. The earliest theoretical studies on this problem were conducted by Tanner and Pipkin [3], for creeping flow of a second-order fluid over a slot, the hole pressure was found to be one quarter of the primary normal-stress difference (N_1). In 1970, Higashitani and Pritchard [4] used a different approach and developed the Higashitani–Pritchard (HP) equation to estimate the hole pressure (P_h):

$$P_h = \int_0^{\tau^b_w} \frac{N_1}{2\tau}\,d\tau \tag{1}$$

where N_1 is the primary normal-stress difference in terms of the shear stress in a simple shear flow, and τ^b_w is the disturbed wall shear stress at point b shown in Fig. 1. For formulating the HP equation, Eq. (1), it was assumed that the streamlines, the shear stress and the axial stress being all symmetrical about the centerline of the slot. As a result, this equation is valid only for creeping flow with low Deborah number (De).

Numerical simulation of the hole pressure problem has been a research topic of considerable interest in recent years. The isothermal simulations were concerned [5,6] with predicting the ratio of hole pressure (P_h) to the primary normal-stress difference (N_1) as a function of Reynolds number Re and Deborah number. Richards and Townsend [7] used the traditional Galerkin finite element method to numerically solve the isothermal hole pressure problem for an implicit Oldroyd-type fluid. Streamline patterns plotted for various flow conditions

* Corresponding author. Tel.: +886-6-2757575x62179; fax: +886-6-2208643.

E-mail address: d1014519@mail.ncku.edu.tw (G.H. Wu).

0017-9310/02/$ - see front matter © 2002 Published by Elsevier Science Ltd.
PII: S0017-9310(02)00144-8

Nomenclature

C_p	heat capacity (kJ/kg °C)	ρ	density (kg/m^3)
De	Deborah number, dimensionless	$\boldsymbol{\tau}$	the viscoelastic stress of the polymer liquid (N/m^2)
$\boldsymbol{d}$	rate-of-deformation tensor (s^{-1})	$\boldsymbol{\tau}_{(1)}$	the upper-convected derivative of the viscoelastic stress $\boldsymbol{\tau}$ (N/m^2 s)
N_1	the primary normal-stress difference (N/m^2)	$\boldsymbol{d}_{(1)}$	the upper-convected derivative of the strain-rate tensor (s^{-2})
P_h	hole pressure (Pa)	$\dot{\boldsymbol{\gamma}}$	shear-rate tensor (s^{-1})
p	pressure (Pa)	$\langle\dot{\gamma}\rangle$	average shear rate (s^{-1})
p_a	pressure at point a (Pa)	$\dot{\gamma}$	shear rate (s^{-1})
P_h^*	dimensionless hole pressure	λ	relaxation time (s)
R	corner radius (m)	ϕ_i	quadratic basic function
$\boldsymbol{s}$	the elastic part of the viscoelastic stress $\boldsymbol{\tau}$ (N/m^2)	ψ_i	bilinear basic function
We	Weissenberg number, dimensionless		
U	average velocity in the channel (m/s)		

Greek symbols

∇	gradient operator (m^{-1})

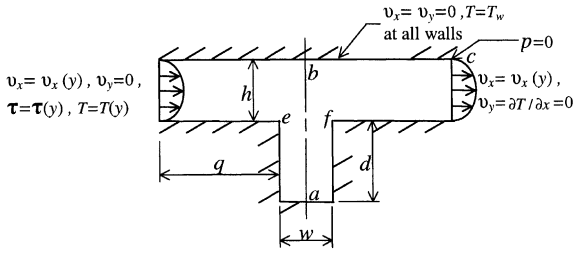

Fig. 1. Flow geometry and boundary conditions.

indicate that both inertia and elasticity bring about an asymmetry in the streamlines. Severe numerical convergence difficulties are encountered when the elasticity of the liquid is increased. Baird and Read [8] used the penalty-Galerkin finite element method to simulate the flow of a polystyrene melt over a rectangular slot perpendicular to the flow direction, values of the stress field predicted by the simulation were compared with those obtained experimentally by means of flow birefringence. The limiting elasticity value as determined by the Weissenberg number (We) for convergence of the algorithm decreased with increased refinement of the mesh. For the case of non-isothermal flow, calculations were conducted by Srinivasan and Finlayson [9], using traditional Galerkin finite element method, they found that the non-isothermal hole pressure is lower than the isothermal hole pressure, and the maximum temperature was predicted at the channel centerline for the highest flow rate ($\langle\dot{\gamma}\rangle = 10$ s^{-1}) in the study.

A few finite element methods have been developed to overcome the convergent difficulties encountered when simulating viscoelastic flow problems. Marchal [10] applied the streamline-upwind/Petrov–Galerkin finite element method to discretize the constitutive equation for elastic-flow problems, and each element was subdivided into a 4×4 subelement for stress analysis. The method showed good behavior for highly elastic-flow problem, but was expensive in terms of computer time. Another method, called the elastic–viscous split-stress (EVSS) finite element method, was proposed by Mendelson [11] in 1983 to simulate the flow of viscoelastic fluids with Newtonian viscosity such as the Oldroyd-B fluids. This method employs the splitting of the extra-stress into its viscous and elastic terms, and a change of variables for the momentum and the constitutive equations, yielding a set of equations involving the velocity $\boldsymbol{v}$, the pressure p, and the new elastic-stress $\boldsymbol{s}$. The rate-of-deformation tensor $\boldsymbol{d}$ is also introduced as an additional unknown, leading to a four-field $(\boldsymbol{v}, p, \boldsymbol{s}, \boldsymbol{d})$ problem. In 1994, the EVSS finite element method incorporating the non-consistent streamline-upwind/Petrov–Galerkin technique (known as the EVSS/SU finite element method) was proposed by Debae [12] and found to be accurate and stable for the viscoelastic flow problems with unsmooth boundaries.

In the present study, the EVSS/SU finite element method is used to simulate the non-isothermal creeping flow of White–Metzner fluids through a channel with a transverse slot. The flow characteristics of the fluid are obtained. Subsequently, the effects of non-isothermal condition, shear-thinning, and slot geometry on hole pressure are investigated.

2. Mathematical modelling

Fig. 1 describes the geometry and boundary conditions of the problem to be analyzed, i.e. a non-isother-

mal creeping flow of a shear-thinning viscoelastic fluid through a channel with a transverse slot. The dimensions are as follows: $h = 7.5$ mm, $q = 32$ mm, $d = 10$ mm, and $w = 4$ mm. The governed equations are as follows:

Continuity equation:

$$\nabla \cdot \boldsymbol{v} = 0 \tag{2}$$

Momentum equation, neglecting body forces:

$$\rho(\boldsymbol{v} \cdot \nabla)\boldsymbol{v} = -\nabla p + \nabla \cdot \boldsymbol{\tau} \tag{3}$$

where $\boldsymbol{\tau}$ is the extra stress.

The total stress tensor is expressed as

$$\boldsymbol{\sigma} = -p\boldsymbol{I} + \boldsymbol{\tau} \tag{4}$$

where p is pressure and $\boldsymbol{I}$ is the unit tensor.

Energy equation, for fluids with constant density ρ, heat capacity C_p, and thermal conductivity k:

$$\rho C_p \boldsymbol{v} \cdot \nabla T = \nabla \cdot k(\nabla T) + \boldsymbol{\tau} : \boldsymbol{d} \tag{5}$$

where $\boldsymbol{d} = (\nabla \boldsymbol{v} + \nabla \boldsymbol{v}^{\mathrm{T}})/2$.

The non-isothermal White–Metzner equation used by Chang [13] to model the non-isothermal flow of nylon-6 is defined by the following equation, together with the curve-fitted parameters and material functions in Table 1.

$$\boldsymbol{\tau} + \lambda \boldsymbol{\tau}_{(1)} = \eta \dot{\boldsymbol{\gamma}} \tag{6}$$

The meaning of each term in Eq. (6) are summarized as follows:

Upper-convective derivative of the extra stress:

$$\boldsymbol{\tau}_{(1)} = \boldsymbol{v} \cdot \nabla \boldsymbol{\tau} - \nabla \boldsymbol{v}^{\mathrm{T}} \cdot \boldsymbol{\tau} - \boldsymbol{\tau} \cdot \nabla \boldsymbol{v} \tag{7}$$

viscosity function: $\eta = \eta(\dot{\gamma}, T)$,
relaxation-time function: $\lambda = \lambda(\dot{\gamma}, T)$.

The relaxation-time function can be obtained via the following equation:

$$\lambda(\dot{\gamma}, T) = \psi_1(\dot{\gamma}, T)/2\eta(\dot{\gamma}, T) \tag{8}$$

where $\psi_1(\dot{\gamma}, T)$ is the primary normal-stress function. The material functions $\lambda(\dot{\gamma}, T)$, $\eta(\dot{\gamma}, T)$ and $\psi_1(\dot{\gamma}, T)$ are all temperature and shear-rate dependent. The shear-rate dependence is described by the Cross model, while the temperature dependence is of the Arrhenius type.

All the velocity and stress are considered to be isothermal fully developed at the inlet. No slip boundary condition is applied at the wall. The wall temperature is constant throughout. Also, the inlet temperature is assumed to be equal to the wall temperature. For the outlet, the velocity is established by solving the problem using the corresponding inelastic generalized Newtonian fluid model with zero normal-force and heat-flux imposed at the outlet.

3. Numerical method

Following the EVSS/SU finite element method proposed by Debae [12], the governing equations for the present flow problem is derived first as follows.

3.1. Dimensionless governing equations in EVSS form

In the EVSS formulation, the viscoelastic stress is split into its elastic and viscous components:

$$\boldsymbol{\tau} = \boldsymbol{s} + 2\eta \boldsymbol{d} \tag{9}$$

where $\boldsymbol{s}$ denotes the elastic component of the viscoelastic stress and $2\eta\boldsymbol{d}$ represents the viscous component.

Upon substituting $(\boldsymbol{s} + 2\eta\boldsymbol{d})$ for $\boldsymbol{\tau}$ into Eqs. (2)–(6), the governing equations in EVSS form become:

$$\nabla \cdot \boldsymbol{v} = 0 \tag{10}$$

$$\boldsymbol{v} \cdot \nabla \boldsymbol{v} = \nabla \cdot (-p\boldsymbol{I} + \boldsymbol{s} + 2\eta \boldsymbol{d}) \tag{11}$$

$$\rho C_p \boldsymbol{v} \cdot \nabla T = \nabla \cdot k(\nabla T) + \boldsymbol{\tau} : \boldsymbol{d} \tag{12}$$

$$\boldsymbol{s} + \lambda(\boldsymbol{s}_{(1)} + 2\eta \boldsymbol{d}_{(1)}) = 0 \tag{13}$$

Table 1
Rheological data and material functions used in the non-isothermal White–Metzner model for nylon-6

$\eta = \eta(\dot{\gamma}, T) = \eta_0(T)\left[1 + (\lambda_1\dot{\gamma})^2\right]^{(n-1)/2}$	$\rho = 986\ \mathrm{kg\,m^{-3}}$
$\eta_0(T) = \eta_{0,\mathrm{ref}} \exp[\beta_1(1/T - 1/T_{\mathrm{ref}})]$	$C_p = 1450\ \mathrm{J\,kg^{-1}\,K^{-1}}$
$\lambda_0(T) = \lambda_{1,\mathrm{ref}} \exp[\beta_2(1/T - 1/T_{\mathrm{ref}})]$	$\mathrm{k} = 0.25\ \mathrm{W\,m^{-1}\,K^{-1}}$
$\eta_0(T_{\mathrm{w}}) = \eta_{0,\mathrm{ref}} = 3687\ \mathrm{N\,s\,m^{-2}}$	$n = 0.7678$
$\psi_1(\dot{\gamma}, T) = \psi_{1,0}(T)\left[1 + (\lambda_2\dot{\gamma})^2\right]^{(n'-2)/2}$	$\beta_1 = 8327\ \mathrm{K}$
$\psi_{1,0}(T) = \psi_{1,0,\mathrm{ref}} \exp[\beta_3(1/T - 1/T_{\mathrm{ref}})]$	$\beta_2 = 17\,300\ \mathrm{K}$
$\lambda_2(T) = \lambda_{2,\mathrm{ref}} \exp[\beta_4(1/T - 1/T_{\mathrm{ref}})]$	$\beta_3 = 18\,630\ \mathrm{K}$
$\psi_{1,0}(T_{\mathrm{w}}) = \psi_{1,0,\mathrm{ref}} = 12.66\ \mathrm{N\,s^2\,m^{-2}}$	$\beta_4 = 5113\ \mathrm{K}$
$\lambda_{1,\mathrm{ref}} = 0.01766\ \mathrm{s}$	$n' = 1.2$
$\lambda_{2,\mathrm{ref}} = 0.1455\ \mathrm{s}$	$T_{\mathrm{w}} = 535\ \mathrm{K}$
$T_{\mathrm{ref}} = 535\ \mathrm{K}$	

$$\boldsymbol{d} - (\nabla \boldsymbol{v} + \nabla \boldsymbol{v}^{\mathrm{T}})/2 = 0 \tag{14}$$

The dimensionless governing equations can be obtained as:

$$\nabla^* \cdot \boldsymbol{v}^* = 0 \tag{15}$$

$$Re\ \boldsymbol{v}^* \cdot \nabla^* \boldsymbol{v}^* = \nabla^* \cdot (-p^* \boldsymbol{I} + \boldsymbol{s}^* + 2\eta^* \boldsymbol{d}^*) \tag{16}$$

$$Pe \boldsymbol{v}^* \cdot \nabla^* T^* = \nabla^{*2} T^* + B_{\mathrm{r}}(\boldsymbol{s}^* + 2\eta^* \boldsymbol{d}^*) : \boldsymbol{d}^* \tag{17}$$

$$\boldsymbol{s}^* + We\lambda^*(\boldsymbol{s}^*_{(1)} + 2\eta^* \boldsymbol{d}^*_{(1)}) = 0 \tag{18}$$

$$\boldsymbol{d}^* - (\nabla^* \boldsymbol{v}^* + \nabla^* \boldsymbol{v}^{*\mathrm{T}})/2 = 0 \tag{19}$$

where the dimensionless variables are defined as follows: $\boldsymbol{x}^* = \boldsymbol{x}/h$, $\boldsymbol{v}^* = \boldsymbol{v}/U$, $\nabla^* = h\nabla$, $\eta^* = \eta/\eta_{0,\mathrm{ref}}$, $T^* = (T - T_{\mathrm{w}})/(T_{\mathrm{b}} - T_{\mathrm{w}})$, $p^* = ph/U\eta_{0,\mathrm{ref}}$, $\boldsymbol{d}^* = h\boldsymbol{d}/U$, and $\boldsymbol{s} = \boldsymbol{s}h/U\eta_{0,\mathrm{ref}}$, while T_{b} is convectively defined as: $T_{\mathrm{b}} = T_{\mathrm{w}} + 1$ (K). Then, the Renolds number, Weissenberg number, Peclet number, and Brinkman number are defined, respectively as:

$$Re = \rho U h/\eta_{0,\mathrm{ref}} \tag{20}$$

$$We = U\lambda_{0,\mathrm{ref}}/h \tag{21}$$

$$Pe = \rho C_p h U/k \tag{22}$$

$$Br = \eta_{0,\mathrm{ref}} U^2/k(T_{\mathrm{b}} - T_{\mathrm{w}}) \tag{23}$$

where $\eta_{0,\mathrm{ref}}$ and $\lambda_{0,\mathrm{ref}}$ are the viscosity and relaxation-time constant at zero-shear rate and at reference temperature.

3.2. Weak formulation of the dimensionless governing equations

The field variables are interpolated within each element by

$$\boldsymbol{v}^* = \sum_{i=1}^{N=8} \phi_i \boldsymbol{v}_i^*, \quad p^* = \sum_{i=1}^{M=4} \psi_i p_i^*, \quad \boldsymbol{s}^* = \sum_{i=1}^{M=4} \psi_i \boldsymbol{s}_i^*,$$
$$\boldsymbol{d}^* = \sum_{i=1}^{M=4} \psi_i \boldsymbol{d}_i^*, \quad T^* = \sum_{i=1}^{N=8} \phi_i T_i^*$$

where $\boldsymbol{v}_i^*$, p_i^*, $\boldsymbol{s}_i^*$, $\boldsymbol{d}_i^*$, T_i^* are nodal values and ϕ_i, ψ_i are quadratic and bilinear basic functions, respectively.

Following the traditional Galerkin's manipulations, the weak form of the dimensionless governing Eqs. (15), (16), and (19) can be derived thereby as

$$\int_\Omega \psi_i (\nabla^* \cdot \boldsymbol{v}^*)\, \mathrm{d}\Omega = 0 \tag{24}$$

$$\int_\Omega \left[\phi_i'(Re\ \boldsymbol{v}^* \cdot \nabla^* \boldsymbol{v}^*) + \nabla^* \phi_i' \cdot (-p^* \boldsymbol{I} + \boldsymbol{s}^* + 2\boldsymbol{d}^*)\, \mathrm{d}\Omega\right] - \int_s \phi_i \boldsymbol{n} \cdot (-p^* \boldsymbol{I} + \boldsymbol{s}^* + 2\boldsymbol{d}^*)\, \mathrm{d}s = 0 \tag{25}$$

$$\int_\Omega \psi_i \left[\boldsymbol{d}^* - (\nabla^* \boldsymbol{v}^* + \nabla^* \boldsymbol{v}^{*\mathrm{T}})/2\right] \mathrm{d}\Omega = 0 \tag{26}$$

The traditional Galerkin method is known to be inappropriate when the convective terms in the hyperbolic constitutive equations become dominant as the Weissenberg number increases. The non-consistent streamline-upwind/Petrov–Galerkin formulation proposed by Debae is therefore applied to constitutive Eq. (18). In this technique, an additional weighing function $(\bar{\boldsymbol{k}}^* \boldsymbol{v}^*/\boldsymbol{v}^* \cdot \boldsymbol{v}^*) \cdot \nabla^* \psi_i$ is applied solely to the convective term $We\lambda^* \boldsymbol{v}^* \cdot \nabla^* (\boldsymbol{s}^* + 2\eta^* \boldsymbol{d}^*)$ of the constitutive equation. The definition of the dimensionless $\bar{\boldsymbol{k}}^*$ can be found in Chang [13], and was originally proposed by Debae. Hence, the following weak form is then obtained:

$$\int_\Omega \Big\{\psi_i \Big[(\boldsymbol{s}^* + We\lambda^*(\boldsymbol{s}^*_{(1)} + 2\eta^* \boldsymbol{d}^*_{(1)})\Big] + (\bar{\boldsymbol{k}}^* \boldsymbol{v}^*/\boldsymbol{v}^* \cdot \boldsymbol{v}^*) \cdot \nabla^* \psi_i [We\lambda^* \boldsymbol{v}^* \cdot \nabla^* (\boldsymbol{s}^* + 2\eta^* \boldsymbol{d}^*)]\Big\}\, \mathrm{d}\Omega = 0 \tag{27}$$

Due to the relatively high Peclet number of this problem, the streamline-upwind Petrov–Galerkin formulation developed by Brooks and Hughes [14] is used to suppress the undesirable oscillations in the calculation of the temperature fields. To solve the equation by this method, an additional weighing function formulation $(\tilde{\boldsymbol{k}}^* \boldsymbol{v}^*/\boldsymbol{v}^* \cdot \boldsymbol{v}^*) \cdot \nabla^* \phi_i$ is applied to all terms of the energy Eq. (17), where $\tilde{\boldsymbol{k}}^*$ is the dimensionless form of $\tilde{\boldsymbol{k}}$ which was proposed by Brooks and Hughes. Consequently, the following weak forms are finally obtained:

$$\int_\Omega \Big\{\phi_i' \Big[Pe \boldsymbol{v}^* \cdot \nabla^* T^* - Br(\boldsymbol{s}^* + 2\eta^* \boldsymbol{d}^*) : \boldsymbol{d}^*\Big] + \nabla^* \phi_i' \cdot \nabla^* T^*\Big\}\, \mathrm{d}\Omega - \int_s \phi_i \boldsymbol{n} \cdot \nabla^* T^*\, \mathrm{d}s = 0 \tag{28}$$

where $\phi_i' = \phi_i + (\tilde{\boldsymbol{k}}^* \boldsymbol{v}^*/\boldsymbol{v}^* \cdot \boldsymbol{v}^*) \cdot \nabla^* \phi_i$.

Since the integrals in Eqs. (24)–(28) are integrals of polynomial functions, they may be readily evaluated numerically using Gaussian quadrature. The above discretization processes lead to a system of non-linear equations of the form

$$\boldsymbol{K}(\boldsymbol{x}^*)\boldsymbol{x}^* = \boldsymbol{f}^* \tag{29}$$

where $\boldsymbol{K}(\boldsymbol{x}^*)$ is global stiffness matrix, $\boldsymbol{f}^*$ is the force vector, $\boldsymbol{x}^* = (v_x^{*(1)} \ldots v_x^{*(n_1)}, v_y^{*(1)} \ldots v_y^{*(n_1)}, s_{xx}^{*(1)} \ldots s_{xx}^{*(n_2)}, s_{yy}^{*(1)} \ldots s_{yy}^{*(n_2)}, s_{xy}^{*(1)} \ldots s_{xy}^{*(n_2)}, d_{xx}^{*(1)} \ldots d_{xx}^{*(n_3)}, d_{yy}^{*(1)} \ldots d_{yy}^{*(n_3)}, d_{xy}^{*(1)} \ldots d_{xy}^{*(n_3)}, p^{*(1)} \ldots p^{*(n_4)}, T^{*(1)} \ldots T^{*(n_5)}$, and n_1, n_2, n_3, n_4, n_5 are respectively the number of velocity, elastic-stress, rate-of-deformation, pressure, and temperature nodal points.

The Newton–Raphson iteration method is employed here to solve the above set of non-linear equations. Due to the sparseness and asymmetry of the global stiffness matrix, the biconjugate gradient stabilized (BiCGStab) method [15] has been developed to compute all the unknowns at each iteration step. Convergence is considered to be achieved when the relative error of each of the dimensionless variables is less than 10^{-4}.

4. Results and discussion

4.1. Test cases

To verify the numerical algorithm, we considered for the flow of an upper-convected Maxwell fluid, a non-shear-thinning case of the melt, past a slot in a channel. The resulting dimensionless hole pressure (P_h^*) is evaluated numerically for various Deborah numbers, and is compared with that derived from the HP theory.

4.1.1. Analytical prediction

For the isothermal fully developed Poiseuille flows, the analytical solutions for the upper-convected Maxwell fluid are:

$$\begin{aligned} \tau_{xy} &= \eta_0 \dot{\gamma} \\ \tau_{xx} &= 2\eta_0 \lambda_0 \dot{\gamma}^2 \\ \tau_{yy} &= 0 \end{aligned} \tag{30}$$

where λ_0 and η_0 are the relaxation-time constant and zero-shear-rate viscosity of this fluid, and $\dot{\gamma}$ is the shear rate of this flow.

The analytical prediction of hole pressure may be obtained by substituting $N_1 = \tau_{xx} - \tau_{yy} = 2\eta_0\lambda_0\dot{\gamma}^2$ and $\boldsymbol{\tau} = \eta_0\dot{\gamma}$ into Eq. (1), and then carrying out the integral by changing the variable from $\boldsymbol{\tau}$ to $\dot{\gamma}$:

$$\begin{aligned} P_h &= \int_0^{\tau_w^b} \frac{N_1}{2\boldsymbol{\tau}}\, d\boldsymbol{\tau} = \frac{N_1}{2}\bigg|_0^{\tau_w^b} - \frac{1}{2}\int_0^{\tau_w^b} \boldsymbol{\tau} d\left(\frac{N_1}{\boldsymbol{\tau}}\right) \\ &= \eta_0\lambda_0(\dot{\gamma}_w^b)^2 - \frac{1}{2}\eta_0\lambda_0(\dot{\gamma}_w^b)^2 = \frac{1}{2}\eta_0\lambda_0(\dot{\gamma}_w^b)^2 \end{aligned}$$

However, the exact value of $\dot{\gamma}_w^b$ is unknown for a given flow. The best way is to obtain this value by numerical simulation. Upon dividing P_h by $\eta_0 U/h$, the dimensionless hole pressure (P_h^*) can be obtained.

4.1.2. Numerical prediction

Numerical simulations are performed for Deborah number ranging from 0 to 4, corresponding to Weissenberg number ranging from 0 to 0.67. The dimensionless Deborah number is an indication of the elasticity of the fluid flow, and defined as:

$$De = \lambda\dot{\gamma}_w \tag{31}$$

where $\dot{\gamma}_w$ is the fully developed wall shear rate in the downstream channel. $De = 6We$ was observed by Malkus [16] for the upper-convected Maxwell fluid in Poiseuille flow. Three finite-element meshes containing 144, 264 and 554 elements (labeled M1, M2, and M3 respectively) are used for the calculations, as shown in Fig. 2. The number of nodes and degrees of freedom (DOF) associated with each mesh are summarized in Table 2.

The results from both the numerical simulation and the theoretical prediction versus Deborah number are shown in Fig. 3. Solutions from mesh M2 and mesh M3 are virtually identical, indicating that mesh M2 is sufficiently fine to obtain reasonable solutions. But mesh M1 seems to be too coarse to produce the same solutions by the other two. The agreement between analytical prediction, Eq. (1) and numerical results by meshes M2 and M3 are excellent for low *De* creeping flow, for which the HP equation holds. This consistency partially validates the reliability of the present code. The deviation is still less than 10% up to a *De* value of about 1.0. For higher *De* values, a larger deviation exists. This is believed to be due to a violation of the assumptions of the HP equation for predicting hole pressure at high *De*.

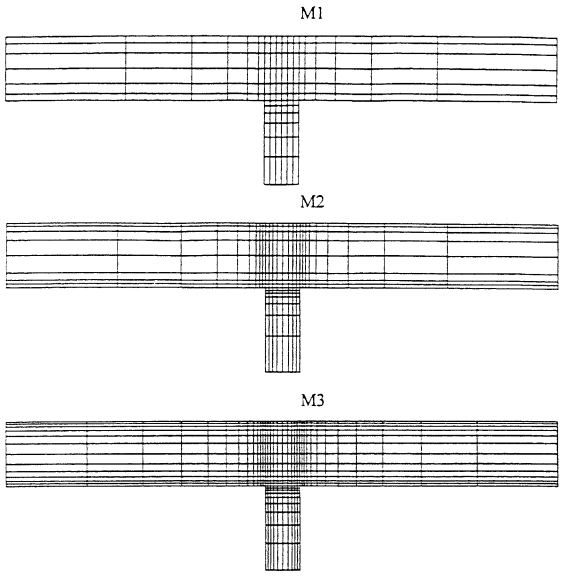

Fig. 2. Meshes used in the current simulation for sharp-corner case: (a) mesh M1; (b) mesh M2; (c) mesh M3.

Table 2
Characteristics of the finite element meshes used

MESH	No. of elements	No. of nodes	No. of DOF
M1	144	637	2499
M2	264	1139	3281
M3	554	2103	5589

4.2. Numerical simulation of the non-isothermal flow of a nylon-6 fluid passing over a transverse slot

The numerical results for the flow of a nylon-6 fluid passing over a transverse slot are presented now. The fluid properties and geometry are fixed, while the average velocity U in the upstream channel is to be variable. The average shear rate is defined as

$$\langle\dot{\gamma}\rangle = U/h$$

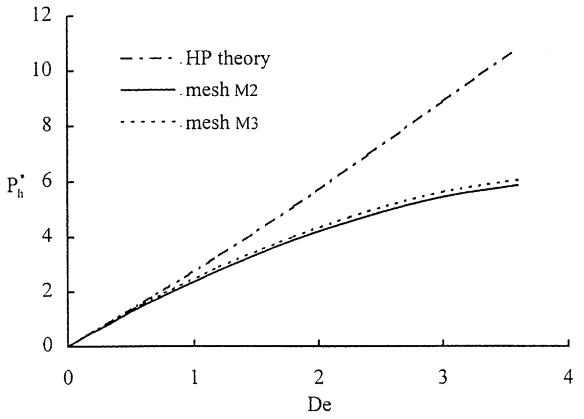

Fig. 3. The results from both the numerical simulation and the theoretical prediction versus *De* number for the upper-convected Maxwell fluid.

Simulations using mesh M2 are performed for the average shear rate $\langle\dot{\gamma}\rangle$ ranging from 0 to 20, corresponding to Weissenberg numbers ranging from 0 to 0.36.

4.2.1. The non-isothermal flow characteristics of the nylon-6 fluid in the channel with sharp corners

Fig. 4 shows comparisons of the dimensionless pressure distributions along the channel walls around the slot for three average shear rates of $\langle\dot{\gamma}\rangle = 1.5$, 6, and 12. A reference pressure of $p = 0$ is imposed at point c as shown in Fig. 1. Along the upper plate of the channel, the pressure distributions are almost linear for the three average shear rates, indicating that it is not much influenced by the presence of the slot. Along the the lower wall of the channel, the pressure decreases gradually from the inlet, then rises as the flow approaches the corner of the slot due to the Weissenberg effect. This behavior, as also observed by Nishimura [17,18] for a polymeric fluid, is more significant for a higher elastic value. Downstream of the slot, the pressure decreases gradually toward the outlet, except in the downstream vicinity of the corner where reversed flow may exit. On the bottom surface of the slot, the pressure is found to be almost a constant value as shown, which decreased for lower Weissenberg number flow.

The corresponding dimensionless temperature contours are shown in Fig. 5, the fluid being subjected to strong shear in the near-wall region due to the relatively high shear rate of the flow. As a result, the temperature rises rapidly in the near-wall region. The dissipation heat is convected downstream with the maximum temperature occurring near the upper wall at the outlet of the channel, due to the high Peclet number of this $\langle\dot{\gamma}\rangle$ range. Hence, the temperature near the channel centerline region is relatively low. Moreover, downstream of the slot,

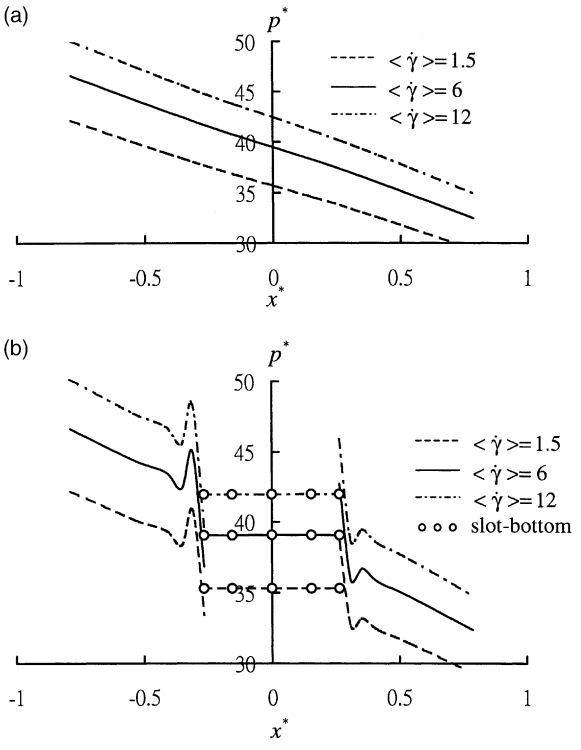

Fig. 4. Comparisons of the dimensionless pressure distributions along the channel walls around the slot: (a) upper plate of the channel; (b) lower wall of the channel and slot bottom.

temperature distribution near the lower plate is a little lower than that near the upper plate, because the flow decelerates more on the lower plate downstream of the slot.

4.2.2. Effects of non-isothermal, shear-thinning, and slot geometry

In an attempt to investigate the non-isothermal effect on hole pressure, the P_h^* values for both isothermal and non-isothermal flows are plotted versus $\langle\dot{\gamma}\rangle$ in Fig. 6. It is clear that temperature-thinning decreases P_h^*, especially at high $\langle\dot{\gamma}\rangle$. The dependence of P_h^* on the slot aspect ratio (d/w) for various $\langle\dot{\gamma}\rangle$ is shown in Fig. 7. The P_h^* value increases with the d/w ratio, and approaches an asymptote for the three average shear rate values. It is believed that this is due to the decrease of the inertia effect. The effect of the rounded corner is investigated with modification of mesh M2 for two rounded-corner cases (dimensionless radius $R^* = 0.05$ and 0.1) (Fig. 8). P_h^* versus $\langle\dot{\gamma}\rangle$ is shown in Fig. 9 for the sharp-corner and the two rounded-corner cases. It can be observed that P_h^* increases with $\langle\dot{\gamma}\rangle$ in all cases. Furthermore, P_h^* is seen to be increased as the corner radius increases for a given value of $\langle\dot{\gamma}\rangle$. This may be believed due to a higher flow rate into the slot when the corner radius gets larger.

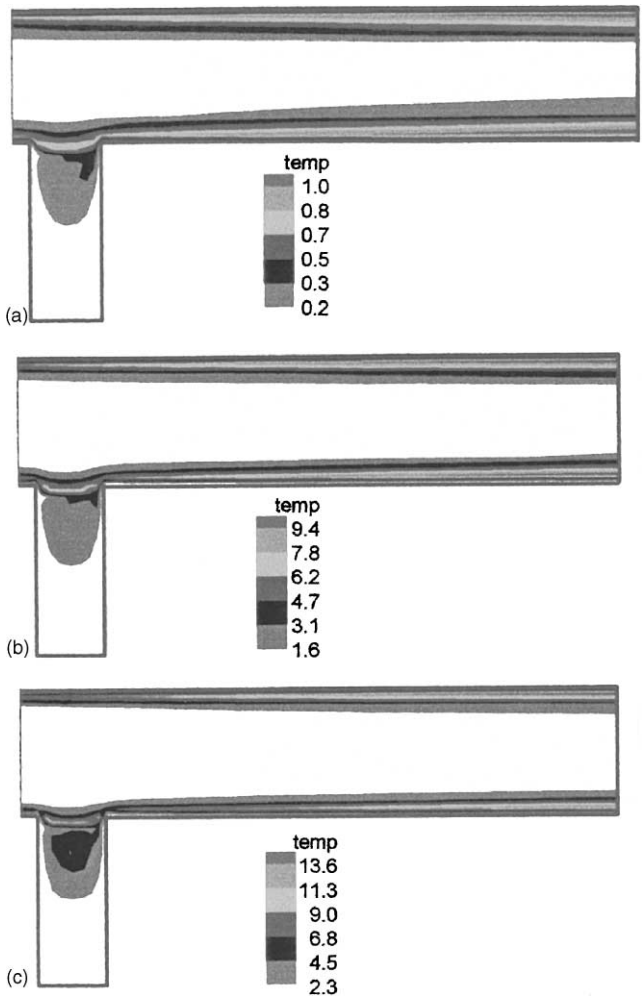

Fig. 5. Partial view of the dimensionless temperature contours for three average shear rates of $\langle\dot{\gamma}\rangle = 1.5, 6.0$ and 12.0. (a) $\langle\dot{\gamma}\rangle = 1.5$; (b) $\langle\dot{\gamma}\rangle = 6.0$; (c) $\langle\dot{\gamma}\rangle = 12.0$.

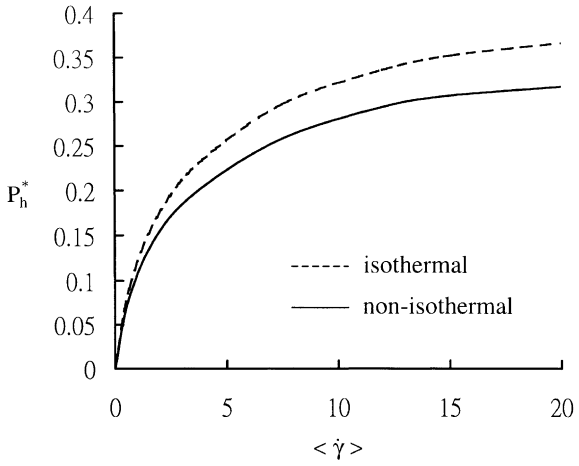

Fig. 6. P_h^* versus $\langle\dot{\gamma}\rangle$ for isothermal and non-isothermal cases.

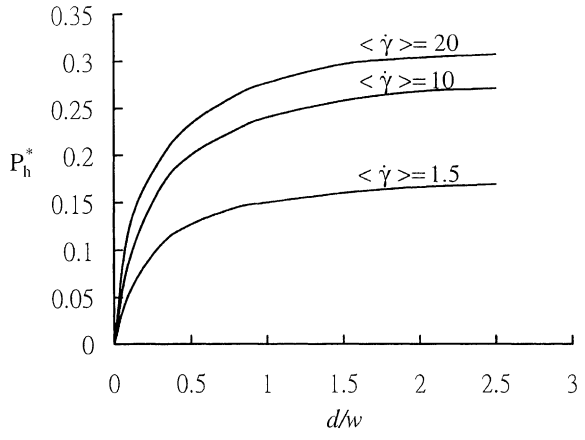

Fig. 7. P_h^* dependence on the slot aspect ratio (d/w) for three $\langle\dot{\gamma}\rangle$ values.

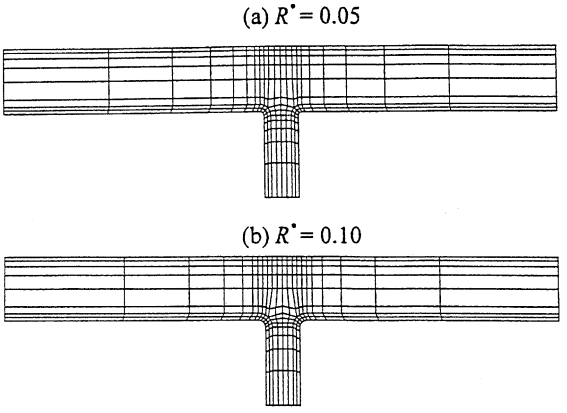

Fig. 8. Meshes used in the current simulation for rounded-corner cases: (a) $R^* = 0.05$; (b) $R^* = 0.1$.

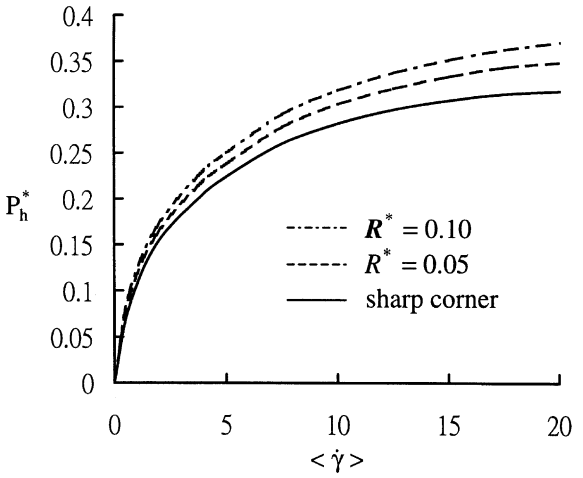

Fig. 9. P_h^* versus $\langle\dot{\gamma}\rangle$ in the current simulation for sharp-corner and two rounded-corner cases.

5. Conclusion

The EVSS/SU finite element method has been employed to solve the non-isothermal hole pressure problem for a nylon-6 liquid. The fluid model used for this flow simulation is a differential-type non-isothermal White–Metzner model, which describes the non-Newtonian behavior of nylon-6. A relatively high Weissenberg number of 0.4 for convergence of the algorithm has been obtained for the sharp-corner case. This is believed to be due to the use of the SU scheme, which is able to smooth out the stress oscillations around the sharp corners where steep stress gradients are present.

Non-isothermal simulation would be necessary when the average shear rate in the channel is significant. A high-temperature flow region is predicted in the near-wall region at the outlet of the channel for the high average shear-rate and high Peclet number of this flow problem, and the temperature in the center line region is relatively low.

The non-isothermal, shear-thinning, and slot geometry effects on hole pressure are investigated. P_h^* increased with $\langle\dot{\gamma}\rangle$ for isothermal viscoelastic flow is a result of the Weissenberg effect. This effect reduces when temperature variation is taken into account. P_h^* increases with the slot aspect ratio and reaches an asymptote for all average shear rates. Rounding off the slot corners will increase P_h^*. The larger the rounding radius, the larger is the predicted P_h^*.

References

[1] R. Bird, R.C. Armstrong, O. Hassager, in: Dynamics of polymeric liquids, vol. 1, John Wiley, 1977.
[2] P. Townsend, A computer model of hole pressure measurement in Poiseuille flow of viscoelastic liquids, Rheol. Acta. 19 (1980) 1–11.
[3] R.I. Tanner, A.C. Pipkin, Intrinsic errors in hole-pressure measurements, Trans. Soc. Rheol. 13 (4) (1969) 471–484.
[4] K. Higashitani, W.G. Pritchard, A kinematic calculation of intrinsic errors in pressure measurements made with holes, Trans. Soc. Rheol. 16 (1972) 687–696.
[5] M.J. Crochet, M. Bezy, Numerical solution for the flow of viscoelastic fluids, J. Non-Newtonian Fluid Mech. 5 (1979) 201–218.
[6] N.R. Jackson, B.A. Finlayson, Calculation of the hole pressure: II. viscoelastic fluids, J. Non-Newtonian Fluid Mech. 10 (1982) 71–84.
[7] G.D. Richards, P. Townsend, A finite element computer model of the hole pressure problem, Rheol. Acta. 20 (1981) 261–269.
[8] D.G. Baird, M.D. Read, Comparison of flow birefringence data with a numerical simulation of the hole pressure, J. Rheol. 32 (6) (1988) 621–683.
[9] R. Srinivasan, B.A. Finlayson, Corrections for the non-isothermal hole pressure problem, J. Non-Newtonian Fluid Mech. 27 (1988) 1–15.
[10] J.M. Marchal, M.J. Crochet, A new mixed finite element for calculating viscoelastic flow, J. Non-Newtonian Fluid Mech. 26 (1987) 77–114.
[11] M.A. Mendelson, P.W. Yeh, R.A. Brown, Finite element calculation of viscoelastic flow in a journal bearing: I. Small Eccentricities, J. Non-Newtonian Fluid Mech. 10 (1982) 31–54.
[12] F. Debae, V. Legat, M.J. Crochet, Practical evaluation for mixed finite element methods for viscoelastic flow, J. Rheol. 38 (2) (1994) 421–442.
[13] R.-Y. Chang, W.-L. Yang, Numerical simulation of non-isothermal extrudate awell at high extrusion rates, J. Non-Newtonian Fluid Mech. 51 (1993) 1–19.
[14] A.N. Brooks, T.J. Hughes, Steamline upwind/Petrov–Galerkin formulation for convection dominated flows with particular emphasis on the incompressible Navier–Stokes equations, Comp. Meth. Appl. Mech. Eng. 32 (1982) 199–259.

[15] H.A. Van der Vorst, BiCGSTAB: a fast and smoothly converging variant of Bi-CG for the solution of nonsymmetric linear system, SIAM J. Sci. Stat. Comput. 13 (1992) 631–644.

[16] D.S. Malkus, M.F. Webster, On the accuracy of finite element and finite difference predictions of non-Newtonian slot pressures for a maxwell fluid, J. Non-Newtonian Fluid Mech. 25 (1987) 93–127.

[17] T. Nishimura, K. Nakamura, A. Horikawa, Two-dimensional viscoelastic flow of polymer solution at channel junction and branch, J. Textile Machinery Soc. Jpn. 33 (1987a) 37–45.

[18] T. Nishimura, K. Nakamura, A. Horikawa, Velocity measurement of viscoelastic flow through a T-shaped junction with a laser doppler velocimeter, J. Textile Machinery Soc. Jpn. 33 (1987b) 105–110.